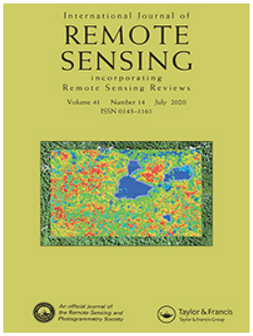

International Journal of Remote Sensing

ISSN: (Print) (Online) Journal homepage: https://www.tandfonline.com/loi/tres20

Detection of soil freeze/thaw states in the Arctic region based on combined SMAP and AMSR-2 radio brightness observations

Konstantin Muzalevskiy & Zdenek Ruzicka

To cite this article: Konstantin Muzalevskiy & Zdenek Ruzicka (2020) Detection of soil freeze/thaw states in the Arctic region based on combined SMAP and AMSR-2 radio brightness observations, International Journal of Remote Sensing, 41:14, 5046-5061, DOI: 10.1080/01431161.2020.1724348

To link to this article: https://doi.org/10.1080/01431161.2020.1724348

INTERNATIONAL JOURNAL OF REMOTE SENSING
2020, VOL. 41, NO. 14, 5046–5061
https://doi.org/10.1080/01431161.2020.1724348

Taylor & Francis
Taylor & Francis Group

Detection of soil freeze/thaw states in the Arctic region based on combined SMAP and AMSR-2 radio brightness observations

Konstantin Muzalevskiy and Zdenek Ruzicka

Laboratory of Radiophysics of the Earth Remote Sensing, Kirensky Institute of Physics Federal Research Center KSC Siberian Branch Russian Academy of Sciences, Krasnoyarsk, Russian Federation

ABSTRACT

In this study, a new approach to identify the freeze/thaw states of tundra topsoil was developed based on the polarization ratio index, which was calculated from the reflectivity values of soil. Reflectivity was estimated from radiometric measurements of the SMAP satellite using the values of vertical polarization brightness temperature measured by the AMSR-2 radiometer at 6.9 GHz; this value was used to characterize the effective temperature of the soil. The proposed approach was tested using weather station data on soil surface temperatures for six test sites located in the North Slope of Alaska and the Yamal Peninsula collected from April 2015 to June 2018. The modified polarization ratio index, calculated from values of reflectivity rather than from brightness temperatures, significantly improved the possibility of determining the reference values of the index in the winter and in the summer. During testing, the modified index showed a good correlation between the dates of transition through the threshold level and soil temperature transition through 0°C, as recorded at meteorological stations.

ARTICLE HISTORY
Received 1 November 2019
Accepted 22 January 2020

1. Introduction

Freeze\thaw and thermal states of permafrost are significant factors determining heat flux and energy balance between the soil surface and atmosphere. They also influence the duration of vegetative cycles, photosynthetic activity of plants, and water and carbon cycles in high-latitude regions. Freeze/thaw (F/T) and thermal states of permafrost are parameter-indicators capable of characterizing the integrated impact of anthropogenic and natural factors on Arctic ecosystems. They were included in the 54 essential climate variables recommended by the World Meteorological Organization for observation (WMO 2015). At the same time, but especially in the Arctic, weather station networks are too sparse to provide enough data about the state of permafrost for climatic models. Modern remote-sensing satellites passing close to polar orbits can observe extensive Arctic areas with high spatial resolution up to several times a day.

CONTACT Konstantin Muzalevskiy rsdkm@ksc.krasn.ru Laboratory of Radiophysics of the Earth Remote Sensing, Kirensky Institute of Physics Federal Research Center KSC Siberian Branch Russian Academy of Sciences, Krasnoyarsk, Russian Federation

At present, an information product of F/T states of soils has been created based on radiometric measurements of the SMAP satellite (Dunbar et al. 2016; Xu et al. 2017). For the SMOS satellite, a similar product has been designed (Rautiainen et al. 2014, 2016), and it is provided through Sodankylä National Satellite Data Centre of Finnish Meteorological Institute. (Similarly, an F/T product based on ASCAT radar data in the C-band is currently in development (Chen, Liu, and Bartsch 2019).) These F/T products are based on the detection of temporal changes in the normalized polarization ratio (NPR) index, which is calculated using brightness temperature (Tb) values. A thresholding approach is then applied to distinguish frozen and thawed soils using reference signatures acquired through the summer and winter (Prince et al. 2018). Using direct measurements of V- and H-polarized brightness temperatures to calculate the NPR leads to spatial errors in the F/T classification for regions where the difference between the reference signatures of Tbs is relatively small or when the NPR dynamic range is reduced. Incorrect classification of F/T soil conditions can be observed during the summer (Prince et al. 2018; Roy et al. 2015), with intensive evaporation and desiccation of topsoil and the additional effects of wave scattering by canopies, as well as in the off-season when soil temperature remains close to zero for long periods, the so-called zero-curtain period (Yi et al. 2019). In the Autumn, the presence of even a thin snow cover on thawed soil can lead to erroneous conclusions about as the presence of frozen soil (Roy et al. 2017a; Schwank et al. 2015). Decreasing physical soil temperature in the winter season leads to erroneous interpretations of frozen state when using a brightness temperature at V polarization for calculation of a frost-factor value; using NPR for calculation of frost-factor value was less prone to retrieval errors caused by very low winter temperatures (Rautiainen et al. 2016). To improve the accuracy of the algorithms for identifying frozen or thawed soil conditions, a set of masks (e.g. air temperature and snow cover) that predict the current time of year for each pixel based on ERA-Interim data European Centre for Medium-Range Weather Forecasts is used (Rautiainen et al. 2016). These data predict soil state relative to weather station measurements of soil or air temperature, with a confidence of more than 80% (Rautiainen et al. 2016; Prince et al. 2018; Roy et al. 2017a).

It is noteworthy that air temperature or soil temperature at a depth of 5 cm or deeper may not be suitable for the validation of remote-sensing F/T products (even in L-band) and is a source of additional inaccuracy. Air temperature and freeze–thaw timing of soil can be decoupled by several factors such as soil canopy (i.e. insulating mosses, vegetation, or snow cover versus bare ground) that shades the soil surface (Smith, Saatchi, and Randerson 2018). Both SMAP and ground-based radiometer measurements indicated freezing conditions when soil temperature sensors installed at 5 cm depth were not frozen (Rowlandson et al. 2018). These errors could possibly be avoided by introducing surface physical temperature directly into the algorithm for estimating emissivity (in place of brightness temperature) (Rautiainen et al. 2016). However, measurements of spatial variations of soil surface temperature within the footprint of an orbiting satellite are globally challenging. Moreover, the temperature of the soil surface may be indirectly estimated using brightness temperature (Holmes et al. 2009; McFarland, Miller, and Neale et al. 1990; Jones et al. 2007). Consequently, quasi-temperature and quasi-emissivity have been used to classify soil conditions as frozen or thawed (Zhao et al. 2011, 2017; Hu et al. 2017; Hu 2019), based on AMSR-E radiometric measurements as the ratio of Tbs at 18.7H/36.5V and Tbs in 36.5V, respectively. The main idea proposed in Zhao et al. (2011, 2017), Hu et al. (2017), and Hu (2019) was to project

a two-dimensional time-series array (quasi-temperature and quasi-emissivity) into a one-dimensional space of a discriminant function using the Fisher approach (Fisher 1936). Then, regression analysis was used to establish a correlation between the discriminant function and soil temperature in the upper 5 cm.

Further development of remote-sensing methods for identifying F/T states of soil may be related to an indirect (through quasi-emissivity) assessment of temperature dependence of permittivity during phase transitions of soil water (Roy et al. 2017b; Mironov and Muzalevskiy 2014). Indeed, it was shown in Mironov and Muzalevskiy (2014), Mironov and Savin (2015), and Mironov et al. (2017) that it is not temperature *per se* but the temperature dependence of complex permittivity that better characterizes the state of the soil. First, due to the influence of latent heat during soil freezing, a zero-curtain period is established, with significant changes in permittivity. However, soil temperature remains almost unchanged for a long time, ranging from −0.5°C to 0°C (Mironov and Muzalevskiy 2014; Mironov and Savin 2015; Mironov et al. 2017). Second, if the total water content in the soil is much higher than the maximum content of unfrozen water, the brightness temperature undergoes significant changes with changes in the sign of soil temperature. These changes in brightness temperature occur due to the phase transition of free liquid soil water into ice (Mironov and Savin 2015; Mironov et al. 2017). This process is accompanied by large changes in the dielectric constant of the soil. In contrast, if the soil is characterized by a high content of unfrozen water (typically for clay or organic soils), and if the total soil moisture does not significantly exceed the maximum content of unfrozen water, then as soil temperature transitions through zero, brightness temperature changes only a little. In this case, the identification of the F/T status of the soil is difficult. Indeed, due to the antiphase changes of emissivity and temperature of frozen soil, variations in brightness temperature may be unchanged. Thus, when the temperature of frozen soil rises, the dielectric constant increases (Mironov et al. 2017) and consequently the emissivity of soil decreases. With decreasing temperature in the freezing soil, the soil permittivity decreases (Mironov et al. 2017) and emissivity increases. As a result of the product of emissivity and soil temperature, the brightness temperature changes only a little. NPR index (Dunbar et al. 2016; Rautiainen et al. 2014, 2016) has eliminated the effect of physical soil temperature in terms of brightness temperature ratios (that leads to ratio of emissivities), but it does not allow to reduce the effects of soil surface roughness and opacity caused by canopy (vegetation or snow).

Consequently, and unlike previous approaches (Dunbar et al. 2016; Rautiainen et al. 2014, 2016), brightness temperature itself is not used in the work described herein; rather, direct reflectivity (estimated from radiometric observations) was used to calculate NPR. Using reflectivity instead of brightness temperature should increase the stability and contrast of the NPR index in the off-season and, during the winter, increase its sensitivity to variations in soil temperature and decrease the influence of soil surface roughness and canopy (vegetation or snow) on the attenuation of soil emission. Unlike previous works (Zhao et al. 2011, 2017; Hu et al. 2017; Hu 2019), we used a combination of low-frequency channels of the radiometers of satellites SMAP and AMSR-2, and the proposed index does not require calibration with respect to soil temperature at test sites. Despite the fact that the temperature dependence of the permittivity is established in laboratory conditions (Mironov and Savin 2015; Mironov et al. 2017), the temperature dependence of reflectivity may not be observed in real remote-sensing conditions on the scale of the footprint, as it

may be smoothed out by other factors. The use of radar data, due to their lack of direct dependence of backscattering coefficient on the effective temperature of the soil, appears preferable for the experimental establishment of such a dependence. Previously, the temperature dependence of the backscattering coefficient, measured by Sentinel-1 and RADARSAT, for mineral soils of moderate latitudes, was examined (Rodionova 2017; Khaldoune et al. 2008). The temperature dependence of reflectivity, which would be measured from space for the Arctic region, has not yet been investigated. The study of this phenomenon, using two tundra test sites, is reported in Section 3 of the current paper. In Section 4, the proposition of a technique for estimating reflectivity from SMAP radiometric data using AMSR-2 data is presented, and the verification of the modified NPR index at several test sites along the Dalton Highway in northern Alaska and in the Yamal Peninsula is described.

2. Test sites (*in-situ* and satellites data)

To study the temperature dependence of reflectivity, Sentinel-1 radar data and radiometric data of the SMAP satellite were used for the test sites in the area of the Isachsen weather station (IS) on the Ellef Ringnes Island and in the area of the Franklin Bluffs weather station (FB) in the North Slope of Alaska (NSA). The Sentinel-1 data at the frequency of 5.4 GHz were selected because Sentinel-1 makes observations in polar regions with a higher frequency all year than the RADARSAT (daily-June–November) or ALOS/PALSAR-2 (not periodically). As a result, Sentinel-1 radar data were used to analyse with an almost daily frequency over the IS weather station. Brief characteristics of the radar on satellite Sentinel-1, radiometers SMAP, and GCOM-W1/AMSR-2 (further used in this article) are summarized in Table 1.

The IS meteorological station was chosen for radar measurements because it is covered with a rare low vegetation (<10 cm, mostly bare soil), and its soil texture is heavy loams or organic soils (Vonlanthen et al. 2005) (having a large amount of bound, unfrozen water content). Due to the small size of land and the mountainous terrain of the IS test site, it was not possible to use the brightness temperature data of the SMAP radiometer (spatial resolution of ~43 km; Table 1). The FB weather station in NSA was selected for brightness temperature measurements, which is sufficiently far from the coastline and from the Brooks Range. Land-cover types of IS and FB and the other test sites in this study are further summarized in Table 2.

SMAP and Sentinel-1 data covered the period from 1 April 2015 to 29 May 2016 and from 22 May 2015 to 19 December 2017, respectively, and were used to study the temperature dependence of reflectivity. Overall, 320 brightness temperatures and 81 radar images were analysed across these periods. Radar backscattering data for the IS

Table 1. Sentinel-1, SMAP, and AMSR-2 satellite's sensor specifications.

	Spatial resolution	Observation angle (°)	Frequency (GHz)
Sentinel-1 (Aulard-Macler et al. 2011)	20 m (EW-HH)	20–47	5.4
SMAP (Piepmeier et al. 2014)	~43 km (H, V)	40	1.4
AMSR-2 (Imaoka et al. 2010)	~48 km (H,V)	55	6.9

Table 2. Land-cover type of test site area.

Test sites	Longitude (°)	Latitude (°)	Percentage of land-cover types (%)
Isachsen (IS)	−103.5500	78.7833	spVe: 63.9%, SnIc:36.1%
Deadhorse (DH)	−148.4653	70.1613	spVe: 48.5%, GrWo: 42.7% Wabd: 3.6%, HeLi: 2.7%
Imnaviat (IM)	−149.3523	68.6397	GrFoSh: 44.5%, spVe: 36.2%, FoSh: 8.1%, miFo: 7.1%, HeLi: 3.8%
Happy Valley (HV)	−148.8483	69.1466	spVe: 53.5%, FoSh: 39.4%, miFo: 5.5%
Franklin Bluffs (FB)	−148.7208	69.6741	spVe: 63.9%, GrWo: 33.5%, Wa: 0.3%, HeLi: 1.1%, GrFoSh: 0.8%
SagMAT/MNT (SG)	−148.6739	69.4330	spVe: 75.3%, FoSh: 13.6%, GrWo: 9.8%
Vaskiny Dachi (VD)	70.2955	68.8835	spVe: 95.4%, Wabd: 1.7%

GrFoSh – Mosaic grassland (50–70%)/forest or shrubland (20–50%);
GrWo – Closed to open (>15%) grassland or woody vegetation on regularly flooded or waterlogged soil – Fresh, brackish, or saline water;
HeLi – Closed to open (>15%) herbaceous vegetation, grassland, savannas, or lichens/mosses;
miFo – Closed to open (>15%) mixed broadleaved and needleleaved forest (>5 m);
FoSh – Mosaic forest or shrubland (50–70%)/grassland (20–50%);
Snlc – Permanent snow and ice.
spVe – Sparse (<15%) vegetation;
Wabd – Waterbodies;
Percentage of land-cover types of the test sites are obtained for a pixel size of 40 × 40 km, for Isachsen – 1 × 1 km.

test site were acquired from GRD Level-1 Sentinel-1 EW (HH-pol medium resolution) products, and the satellite pass was at about 14:00 (UTC). Radar images were processed in the Sentinel Application Platform (SNAP) according to the standard procedure: applying precise orbits, thermal noise removal, radiometric calibration, speckle filtering (3 × 3 mean filter), range Doppler terrain correction (ACE2_5 min digital elevation model with UTM Zone 13 projection), and incidence angle normalization (reference angle 40°). Brightness temperature data were acquired from an enhanced Level-1C SMAP product (SPL1CTB_E) ascending half-orbit passes (aft looking antenna scan).

For the extensive period of testing the new F/T approach, SMAP and AMSR-2 data were used from April 2015 to June 2018 over an extended number of test sites: Deadhorse (DH), FB, SagMAT (SG), Happy Valley (HV), Imnaviat (IM), and Vaskiny Dachi (VD), located in NSA and Yamal Peninsula, respectively. A map of locations and land-cover characteristics of the test sites are shown in Figure 1 and Table 2, respectively. Both SMAP and GCOM-W1 /AMSR-2 observations occurred for ascending orbits. The territory of the selected test sites contained a significant variety of landscapes: typical Arctic tundra, tundra, and forest-tundra, which allowed for a comprehensive assessment of the applicability of the proposed approach for typical lands in polar regions.

3. Temperature dependence of the reflectivity of tundra soils

Theoretical analysis of brightness temperature variations of the tundra soil was performed using the following model for a dielectrically homogeneous isothermal medium (Wigneron et al. 2017):

$$\mathrm{Tb}_{p1.4} = \left[1 - \Gamma_p\right] \times T_s,\ \Gamma_p = \left|R_p(\varepsilon_s)\right|^2 e^{-\mathrm{TH}}. \quad (1)$$

Here, p = H and p = V signify horizontal and vertical polarizations, T_s is the effective soil temperature, Γ_p is the reflectivity, $R_p(\vartheta, \varepsilon_s)$ is the Fresnel reflection coefficient, $\varepsilon_s = \varepsilon_s(\rho_d, m_v, T_s, C)$

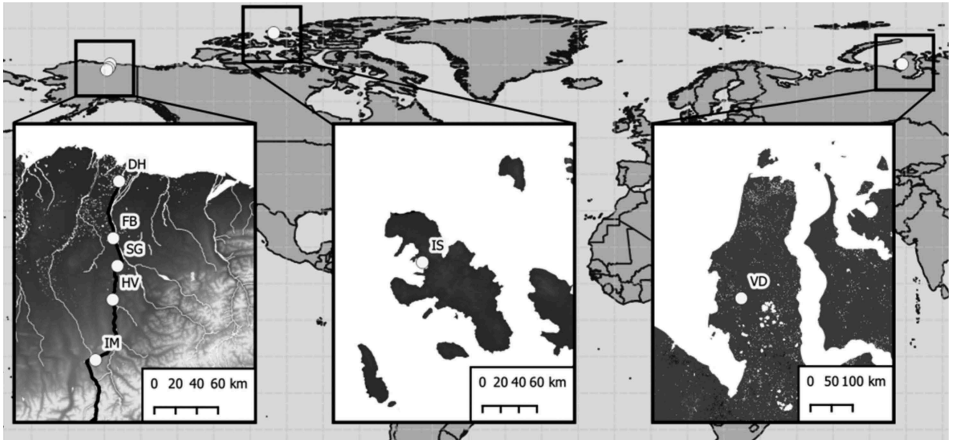

Figure 1. Location map of test sites.

is the soil complex permittivity, ρ_d is the soil bulk dry density, m_v is the volumetric soil moisture, C is the soil texture factor (clay or organic content), and TH is the combined parameter of vegetation (snow) optical depth and roughness according to Parrens et al. (2016; see formula (7)). To analyse variations of backscattering, Oh's model was used under the assumption of a dielectrically homogeneous active topsoil (Oh, Sarabandi, and Ulaby 1992):

$$\sigma_{HH} = g\sqrt{p}\cos^3\vartheta[R_V(\vartheta,\varepsilon_s) + R_H(\vartheta,\varepsilon_s)],$$

$$g = 0.7\left(1 - e^{-0.65k_0 h_r{}^{1.8}}\right), \tag{2}$$

$$\sqrt{p} = 1 - (2\vartheta/\pi)^{0.314/R_0(\varepsilon_s)} e^{-k_0 h_r},$$

where ϑ is the incidence angle in radians, $R_0 = |R_{H,V}(\vartheta = 0)|^2$, k_0 is a free space wave number, and h_r is the root-mean-square deviation of the soil surface height. In applying Equations (1) and (2), we neglected wave scattering by vegetation and snow cover, and we did not consider the profiles of the permittivity and temperature in the active layer of frozen soil.

The temperature dependence of the radar backscattering coefficient measured by Sentinel-1 and reflectivity measured by SMAP (estimated from Equation (1), using values of surface soil temperature) are depicted in Figures 2 and 3, respectively, for the FB and IS test sites. Soil temperature data were provided (UAA 2019). For both test sites, variations in the backscattering coefficient and reflectivity were approximately 4–5 dB in the range of soil surface temperature changes from −30°C to 0°C (Figures 2 and 3). However, it is necessary to demonstrate whether it is possible, using models (1) and (2), to theoretically describe that the temperature dependence of reflectivity is due only to variations in temperature-induced changes in soil permittivity or whether the observed changes were caused by other phenomena.

To achieve this, using experimental observations and emission and scattering models (1)–(2), a permittivity model of organic soil (Mironov and Savin 2015), the inverse problems for the FB and IS test sites were solved relative to moisture content, density, and soil

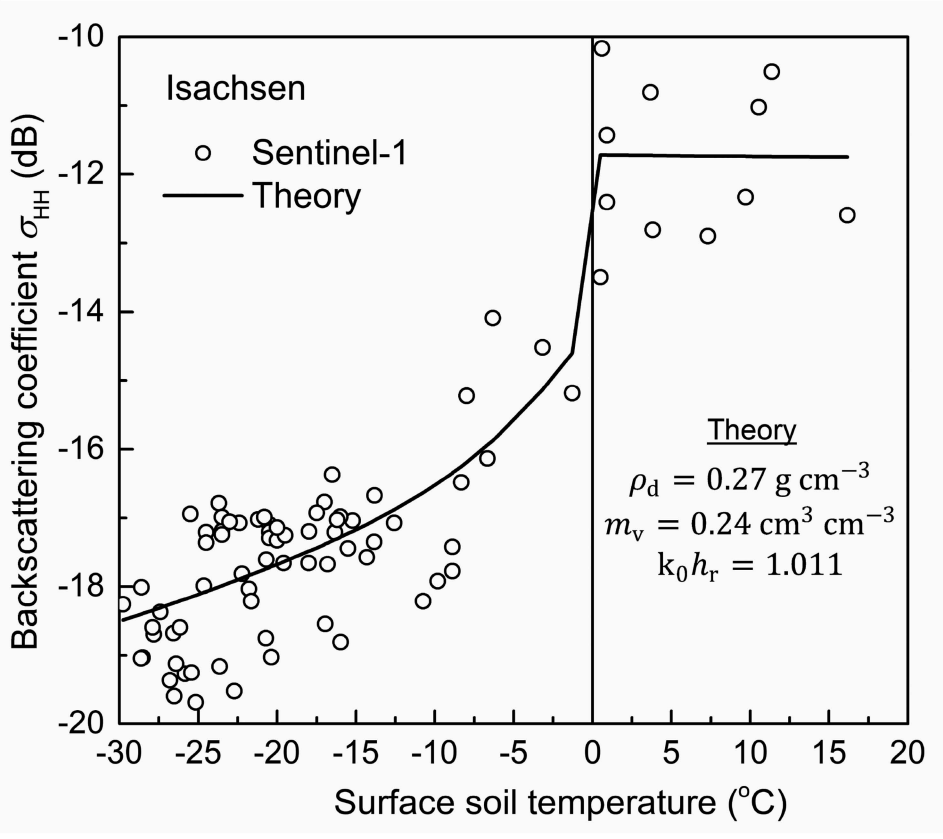

Figure 2. Dependence between the Sentinel-1 backscattering coefficient and the soil surface temperature (0–1 cm) in the area of IS weather station.

surface roughness (radar case only). The two inverse problems were solved for all available data while minimizing the residual norm between the time series of brightness temperatures measured by the SMAP radiometer and calculated values and between the time series of the backscattering coefficient measured by Sentinel-1 and the calculated values. Backscattering coefficients were calculated by neglecting the frequency dispersion of the complex dielectric permittivity in the frequency range from 1.4 to 5.4 GHz. The time-series data were taken for the whole year, thereby including both thawed and frozen soil states. The calculated reflection and backscattering coefficients for the optimally found parameters, during the minimization process as a function of soil surface temperature, are shown in Figures 2 and 3. The retrieved values of the soil bulk dry density corresponded well with the bulk dry density of the organic topsoil observed in natural conditions in the Arctic tundra. The average soil moisture of ~0.3 cm^3 cm^{-3} measured by the IS weather station at a depth of 11 cm in the period 2015–2016 was close to the retrieved soil moisture value (0.24 cm^3 cm^{-3}) from Sentinel-1 observations. The average soil moisture of ~0.4 cm^3 cm^{-3}, measured by the FB weather station at a depth of 18–22 cm in the period 2015–2016, was slightly lower than the retrieved soil moisture value from SMAP observations.

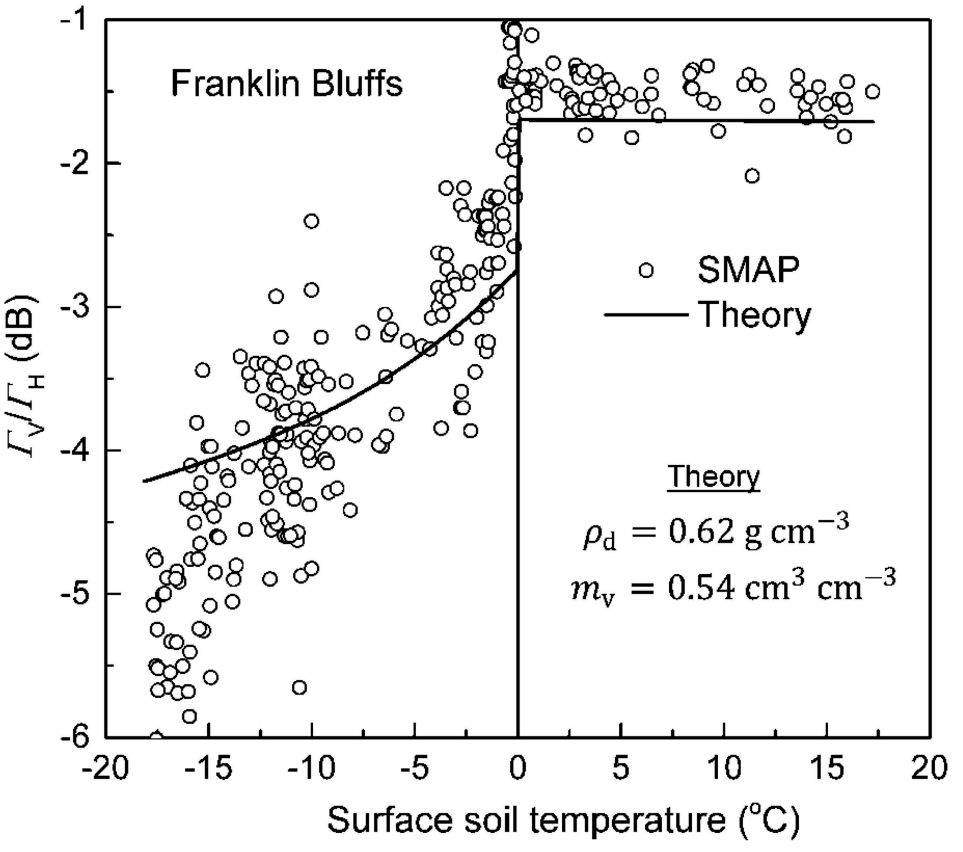

Figure 3. Dependence between the ratio of reflectivities and soil surface temperature. (To minimize the effects associated with wave attenuation in the snow and vegetation cover and also due to scattering on the soil surface roughness, the ratio reflectivities V/H were calculated.)

The values of root-mean-square deviations of the soil surface heights (h_r = 0.9 cm) corresponded to a flat landscape in the vicinity of the IS weather station. The correlation coefficient between the measured and retrieved values of the reflectivity polarization ratio (Figure 2) and backscattering coefficient (Figure 3) in the negative temperature region were 0.68 and 0.73, respectively. The most significant deviations of the measured value of reflectivity and backscattering coefficient from the calculated values were observed in the temperature range −30°C to −10°C. The gradients of permittivity and temperature observed at this time in the active topsoil contributed significantly to the emission and scattering, and these were not taken into account in models (1) and (2). Note that the phenomenon of temperature dependence of the scattering cross section and reflectivity is observed at different scales of spatial averaging of Sentinel-1 (~20 m) and SMAP (~43 km), with respect to the reference point measurements of weather stations (Figures 2 and 3). It can be concluded that the temperature dependence of the backscattering coefficient and reflectivity for Arctic tundra soil can be described with a good degree of accuracy only due to temperature changes in the permittivity of the organic-rich topsoil. Indeed, as the soil temperature passed through 0, free water contained in the soil freezes and turns into ice (or the ice

melts into free water), and these phase transitions result in a jump of the reflectivity of only 1.5 dB (see Figures 2 and 3). If the temperature in the freezing soil decreased, a part of the unfrozen water (consisting of bound water that never freezes and a transitional one that undergoes phase transformations) passes into the ice by infinitesimal fractions, and this is accompanied by a monotonic decrease in the permittivity and consequently in the soil reflectivity too (With increasing temperature of the frozen soil, this process is reversed.) The experimentally confirmed temperature dependence derived from satellite observations opens up the possibility of a more accurate approach to identifying frozen and thawed soil states based on the measurement of reflectivity.

The following section describes an approach for identifying the thawed and frozen states of soil cover based on estimates of soil reflectivity from SMAP and AMSR-2 radiometric data that have a close spatial resolution (see Table 1).

4. A new approach for the determination of freeze/thaw soil status

First of all, consider the variations in the NPR index calculated using brightness temperature values measured by SMAP at six test sites: DH, FB, SG, HV, IM, and VD. Histograms of the NPR distributions from 1 April 2015 to 31 December 2017 are shown in Figure 4. For all test sites other than DH, NPR values exhibited distributions with one maximum. It does not allow us to distinguish between the reference values of NPR for winter and that for summer. Hence, successful classification of the frozen and thawed states of soils is difficult. The reasons for this behaviour of NPR, calculated on the basis of direct values of brightness temperatures, are described in the Introduction. For better separation of the reference values of NPR, a modified MPR is proposed, which is calculated on the basis of reflectivity values:

$$\mathrm{MPR} = \frac{1}{2}\frac{\Gamma_{\mathrm{H}} + \Gamma_{\mathrm{V}}}{\Gamma_{\mathrm{H}} - \Gamma_{\mathrm{V}}} \tag{3}$$

The authors believe that the calculation of the MPR index based on reflectivity should minimize the influence of canopy, since in this case, in formula (3), the parameter TH is cancelled. On the contrary, the use of emissivity in calculating the index MPR leaves dependent on TH. The values of Γ_{H} and Γ_{V} can be estimated using a simple model (1), but it is necessary to know the soil temperature in each pixel, which cannot be provided by ground-based weather stations. MODIS LST data correlate better with the temperature of air, rather than soil temperature (Hachem, Duguay, and Allard et al. 2012). However, the radio brightness temperature on vertical polarization, $\mathrm{Tb}_{\mathrm{V6.9}}$, measured by AMSR-2 at a frequency of 6.9 GHz, is highly correlated to the temperature of tundra soil (Muzalevskiy et al. 2016). The physical basis for this effect is the observation angle of the AMSR-2 radiometer, which is close to the Brewster angle (55°), and this leads to a decreased impact of reflectivity Γ_{V} on measured brightness temperature $\mathrm{Tb}_{\mathrm{V6.9}}$. As a result, and as expected from model (1), Tb becomes mainly directly proportional to soil temperature. By putting $T_s \sim \mathrm{Tb}_{\mathrm{V6.9}}$ in Equation (1), we arrive at a simple estimate for Γ_p as quasi-reflectivity, where p= H and p= V

$$\Gamma_p = 1 - Tb_{p1.4}/\mathrm{Tb}_{\mathrm{V6.9}} \tag{4}$$

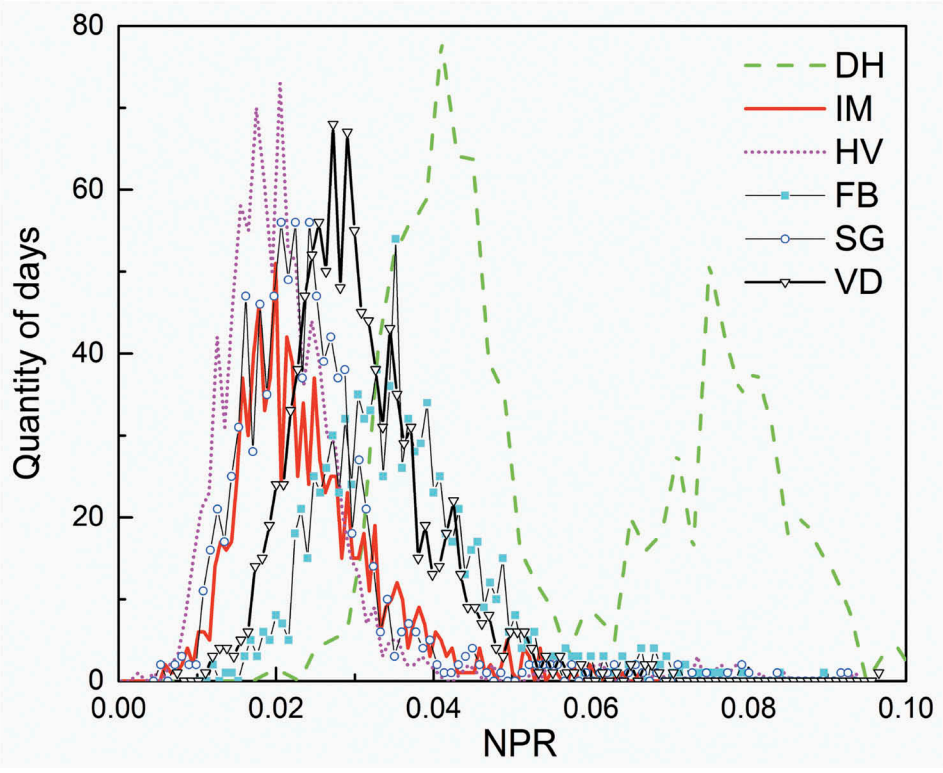

Figure 4. Distribution of NPR values in a period of 3 years (2015–2018), calculated from SMAP brightness data, for six test sites.

where $Tb_{p1.4}/Tb_{V6.9}$ is the quasi-emissivity, which were proposed in Zhao et al. (2011) for 18.7H and 36.5V frequencies. On the basis of formulas (3) and (4) for all test sites, MPR calculations were performed for the period from April 2015 to June 2018. As an example, in Figure 5, histograms of the MPR index exhibit two maximum distributions for HV and FB test sites. Temperature dependence of MPR index for all test sites is shown in Figure 6. Reference values of MPR were well identified in the region of positive and negative temperatures, with a threshold level equal to ~1.2 (Figures 5 and 6). The proposed MPR index, for all test sites, demonstrated a significant separation of the reference MPR values for winter and summer and allowed successful classification of frozen and thawed soil states. Application of the proposed MPR index from spring 2015 to spring 2018 resulted in the correct identification of soil F/T states at all test sites. Figure 7 presents the results of the comparison between the times of the transition of the MPR index through the threshold level equal to ~1.2 with respect to the point in time when, according to weather station data, the soil surface temperature transitioned through 0°C. The time series of the MPR index and the soil surface temperature were averaged using a 7-day moving average window.

In the spring time, the MPR index on ~12 days earlier characterizes the soil as thawed. In the autumn time, the MPR index on ~7 days later characterizes the soil as frozen. During the spring, due to the shielding effect of thawing snow cover, at frequencies of 1.4 GHz

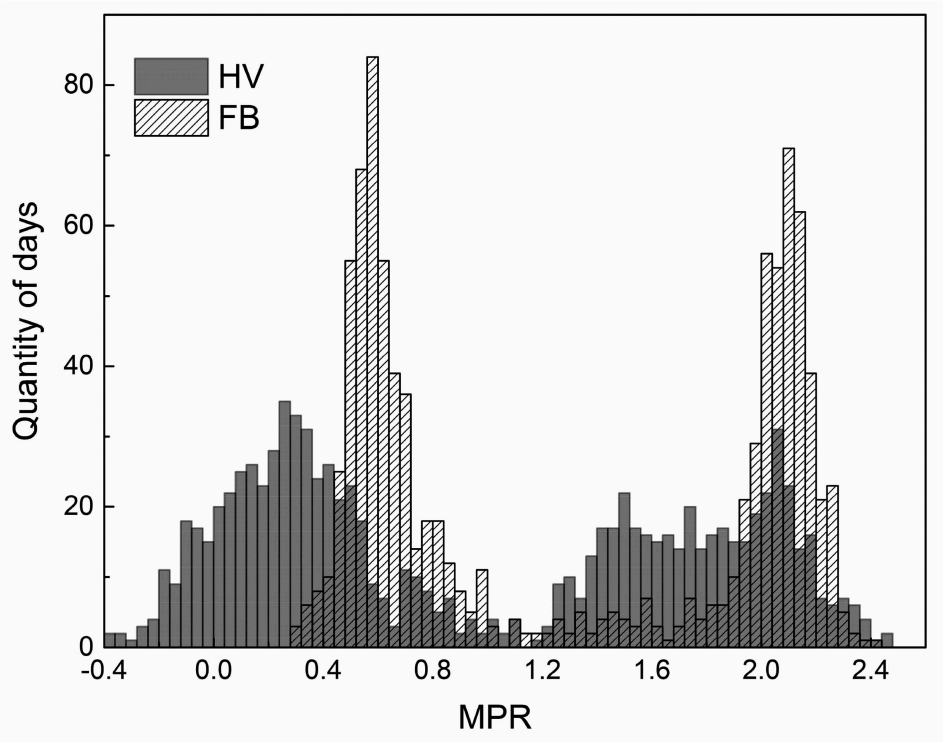

Figure 5. Distribution of MPR index in a period of 3 years (2015–2018), calculated from SMAP brightness data, for HV and FB test sites.

and higher, it is impossible to detect the contribution of the underlying soil layers to the brightness temperature. Field experiments have demonstrated that liquid water within snow dramatically increased the Tbs, resulting in false retrievals of the occurrence of soil thaw events (Roy et al. 2017a, 2017b). As a result, the thawed state of the soil, based on satellite measurements, is deemed to have occurred earlier than the contact soil surface temperature measurements (Figure 7). Because of differing conditions of snow accumulation and melting within each pixel at different sites, there was a low coefficient of determination (R^2 = 0.38) between the time of soil thawing defined by the weather station and the timing according to satellite data (Figure 7). However, despite the diversity of the landscape including vegetation cover and relief within each pixel, there is a high coefficient of determination (R^2 = 0.77) between the date of soil freezing derived from satellite observations and the date derived from weather station data (Figure 7). For the DH test site during the fall period, the MPR index characterized the soil as frozen a little later than for other test sites (see Figure 7). This reflects the later freezing of wetlands, including open water and regularly flooded/waterlogged areas. In the vicinity of the DH meteorological station, such areas accounted for up to 46.3% of the pixel area, unlike other test sites (see Table 2). The approach described in this article does not allow identification of the F/T state of soil separately from waterbodies. The contribution of waterbodies to the total radio brightness temperature can be taken into account when the percentage of the total area of each pixel is known. However, in the autumn, this

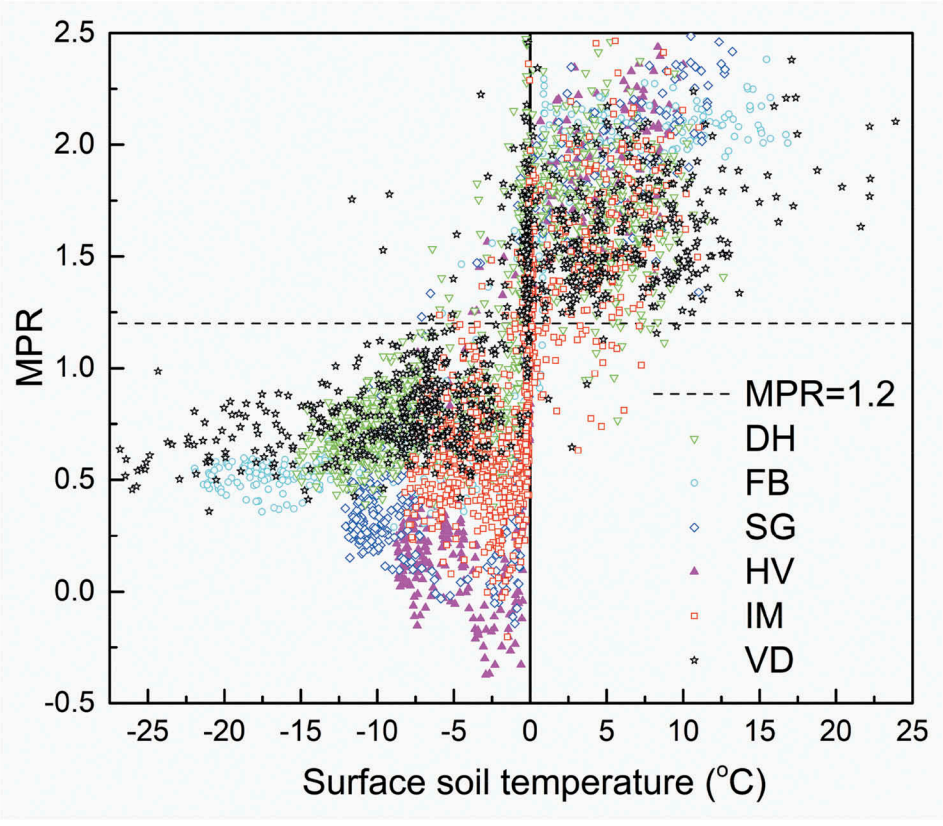

Figure 6. Modified value of the polarization index as a function of the surface soil temperature (at the depth of ~1 cm) for six test sites.

requires the development of a model of ice thickness growth on waterbodies with the necessary set of additional data on air temperature, wind speed, and snow cover thickness, which makes the task very complex and difficult. Consequently, the proposed approach allows identification of the F/T state of soil if the proportion of waterbodies is such that their contribution to the total brightness temperature may be neglected. If the proportion of waterbodies (or waterlogged soil) is significant (not less than 46.3%, as for the DH test area), then the proposed approach allows identification of the F/T state of the entire underlying surface.

5. Conclusions

In this paper, the temperature dependences of reflectivity, measured by a SMAP radiometer, and the backscattering coefficient, measured by Sentinel-1, during the heating and cooling of frozen soil were determined. Two typical tundra test sites located in the North Slope of Alaska near Franklin Bluffs meteorological station and on Ellef Ringnes Island near Isachsen weather station were investigated. In the range of soil surface temperature from −30°C to 0°C, variations of the backscattering coefficient and reflectivity were approximately 4–5 dB for both test sites. These changes were mainly due to the

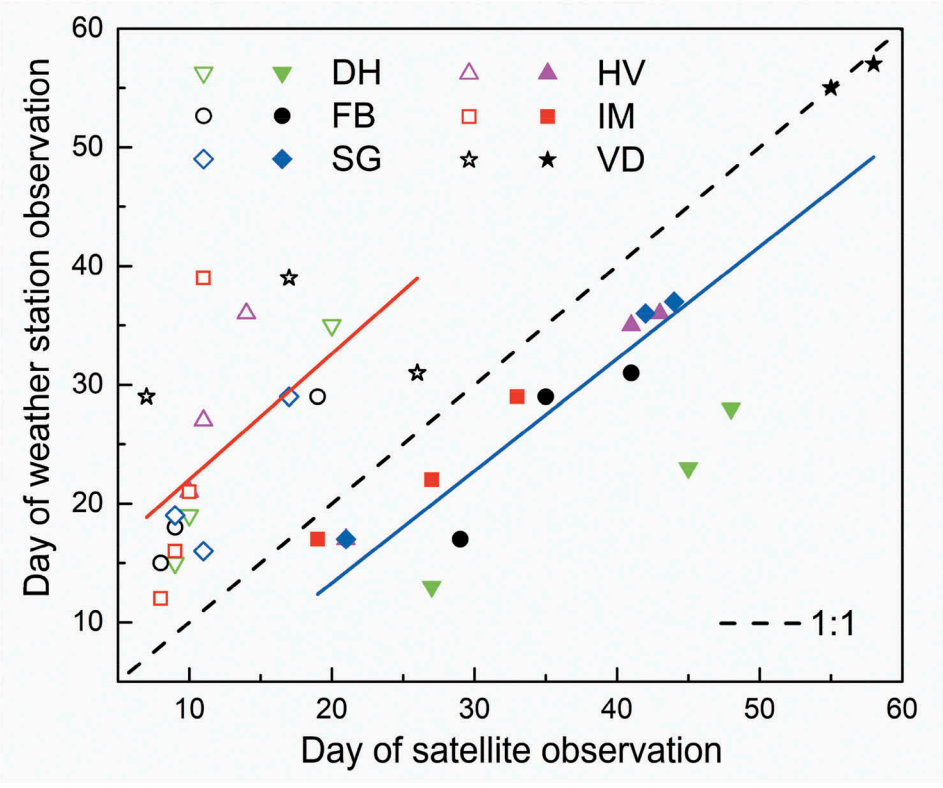

Figure 7. Detection of soil state status based on weather station versus satellite data. Axes scales are marked up in calendar days from 1 May in the spring and from 1 September in the autumn. The open and filled symbols stand for spring and autumn time, respectively. Solid lines are marked linear regressions to the experimental data. The results of the linear regression for the spring and autumn time were $R^2 = 0.38$, RMSE = 7.1 days and $R^2 = 0.77$, RMSE = 6.4 days, respectively.

temperature dependence of soil permittivity for soils with a high content of organic matter. The established temperature dependences of reflectivity made it possible to propose a new approach for the classification of the frozen and thawed states of tundra soil based on the polarization ratio index. The novelty of the proposed approach lies in the method for estimating reflectivity of soil from SMAP radiometric data using the values of V-polarized brightness temperature measured by the AMSR-2 radiometer at 6.9 GHz to characterize the effective temperature of the topsoil. The polarization ratio index, calculated from reflectivity values, rather than the polarization ratio index calculated using brightness temperature values, significantly improved the possibility of determining the reference values of frozen and thawed soil states. Soil F/T states, determined using the modified index from SMAP and AMSR-2 satellite measurements, corresponded to F/T states determined using *in-situ* soil temperature measurements. Further work will be aimed at additional validation of the proposed approach, using a wider range of test sites, including both tundra and medium latitude areas.

Disclosure statement

No potential conflict of interest was reported by the authors.

Funding

This study was funded by the SB RAS Program (project No. 0356-2019-0004).

References

Aulard-Macler, M., Barstow, R., Ramsbottom, D., Lim, P. 2011. "Sentinel-1 Product Definition." In *MacDonald, Dettwiler and Associate, SEN-RS-52-7440*, 129.

Chen, X., L. Liu, and A. Bartsch. 2019. "Detecting Soil Freeze/Thaw Onsets in Alaska Using SMAP and ASCAT Data." *Remote Sensing of Environment* 220: 59–70. doi:10.1016/j.rse.2018.10.010.

Dunbar, S., X. Xu, A. Colliander, C. Derksen, J. Kimball, and Y. Kim. 2016. "Algorithm Theoretical Basis Document (ATBD). SMAP Level 3 Radiometer Freeze/Thaw Data Products." *JPL CIT: JPL D-56288* 33.

Fisher, R. A. 1936. "The Use of Multiple Measurements in Taxonomic Problems." *Annals of Eugenics* 7: 179–188. doi:10.1111/j.1469-1809.1936.tb02137.x.

Hachem, S., C. R. Duguay, M. Allard. 2012. "Comparison of MODIS-derived Land Surface Temperatures with Ground Surface and Air Temperature Measurements in Continuous Permafrost Terrain". *The Cryosphere* 6: 51–69. doi:10.5194/tc-6-51-2012.

Holmes, T. R., R. A. M. De Jeu, M. Owe, A. J. Dolman. 2009. "Land Surface Temperatures from Ka-band (37 GHz) Passive Microwave Observations." *Journal of Geophysical Research* 114 (D04113). doi:10.1029/2008JD010257.

Hu, T. 2019. "A Continuous Global Record of Near-surface Soil Freeze/thaw Status from AMSR-E and AMSR2 Data." *International Journal of Remote Sensing* 40 (18): 6993–7016. doi:10.1080/01431161.2019.1597307.

Hu, T., T. Zhao, J. Shi, S. Wu, D. Liu, H. Qin, and K. Zhao. 2017. "High-Resolution Mapping of Freeze/Thaw Status in China via Fusion of MODIS and AMSR2 Data." *Remote Sensing* 9: 1339. doi:10.3390/rs9121339.

Imaoka, K., Kachi, M., Kasahara, M., Ito, N., Nakagawa, K., Oki, T. 2010. "Instrument Performance and Calibration of AMSR-E and AMSR2." *International Archives of the Photogrammetry, Remote Sensing and Spatial Information Science* XXXVIII (8): 13–16.

Jones, L. A., Kimball, J.S., McDonald, K.C., Chan, S.T.K., Njoku, E.G., Oechel, W.C. 2007. "Satellite Microwave Remote Sensing of Boreal and Arctic Soil Temperatures from AMSR-E." *IEEE Transactions on Geoscience and Remote Sensing* 45 (7): 2004–2018. doi:10.1109/TGRS.2007.898436.

Khaldoune, J., Bochove, E., Bernier, M., Nolin, M.C. 2008. "An Approach for Mapping Frozen Soil of Agricultural Land under Snow Cover Using RADARSAT-1 and RADARSAT-2." *IEEE Geoscience and Remote Sensing Symposium Proceeding, Boston*, 3: III-382–III-385.

McFarland, M. J., R. L. Miller, C. M. U. Neale. 1990. "Land Surface Temperature Derived from the SSM/I Passive Microwave Brightness Temperatures." *IEEE Transactions on Geoscience and Remote Sensing* 28 (5): 839–845. doi:10.1109/36.58971.

Mironov, V. L., L. G. Kosolapova, Y. I. Lukin, A. Y. Karavaysky, and I. P. Molostov. 2017. "Temperature- and Texture-dependent Dielectric Model for Frozen and Thawed Mineral Soils at a Frequency of 1.4GHz." *Remote Sensing of Environment* 200: 240–249. doi:10.1016/j.rse.2017.08.007.

Mironov, V. L., and K. V. Muzalevskiy. 2014. "[Method for Measuring the Temperature Dependence of the Topsoil Permittivity on the Yamal Peninsula Using MIRAS SMOS Radiometer Data]." In *Proceedings of the Conference of regional problems of remote sensing of the Earth*, 186–189. Krasnoyarsk. (in russian). [online]. http://rprs.sfu-kras.ru/sites/default/files/v_pechat_-materialy_mezhdunarodnoy_nauchnoy_konferencii.pdf

Mironov, V. L., and I. V. Savin. 2015. "A Temperature-dependent Multi-relaxation Spectroscopic Dielectric Model for Thawed and Frozen Organic Soil at 0.05–15 GHz." *Physics and Chemistry of the Earth* Parts A/B/C (83–84): 57–64. doi:10.1016/j.pce.2015.02.011.

Muzalevskiy, K. V., Z. Ruzicka, L. G. Kosolapova, and V. L. Mironov. 2016. "Temperature Dependence of SMOS/MIRAS, GCOM-W1/AMSR2 Brightness Temperature and ALOS/PALSAR Radar Backscattering at Arctic Test Sites." In *Progress in Electromagnetic Research Symposium (PIERS)*, 3578–3582. Shanghai.

Oh, Y., K. Sarabandi, and F. T. Ulaby. 1992. "An Empirical Model and an Inversion Technique for Radar Scattering from Bare Soil Surfaces." *IEEE Transactions on Geoscience and Remote Sensing* 30 (2): 370–381. doi:10.1109/36.134086.

Parrens, M., J.-P. Wigneron, P. Richaume, A. Mialon, A. Al Bitar, R. Fernandez-Moran, A. Al-Yaari, et al. 2016. "Global-scale Surface Roughness Effects at L-band as Estimated from SMOS Observations." *Remote Sensing of Environment* 181: 122–136. doi:10.1016/j.rse.2016.04.006.

Piepmeier, J., Mohammed, P., Amici, G., Kim, E., Peng, J., Ruf., C. 2014. "Algorithm Theoretical Basis Document (ATBD), SMAP Calibrated, Time-Ordered Brightness Temperatures L1B_TB Data Product." *NASA, JPL, Revision A,* 83.

Prince, M., A. Roy, L. Brucker, A. Royer, Y. Kim, T. Zhao. 2018. "Northern Hemisphere Surface Freeze–Thaw Product from Aquarius L-band Radiometers." *Earth System Science Data* 10: 2055–2067. doi:10.5194/essd-10-2055-2018.

Rautiainen, K., J. Lemmetyinen, M. Schwank, A. Kontu, C. B. Ménard, C. Mätzler, M. Drusch, et al. 2014. "Detection of Soil Freezing from L-band Passive Microwave Observations". *Remote Sensing of Environment* 147: 206–218. doi:10.1016/j.rse.2014.03.007.

Rautiainen, K., T. Parkkinen, J. Lemmetyinen, M. Schwank, A. Wiesmann, J. Ikonen, C. Derksen, et al. 2016. "SMOS Prototype Algorithm for Detecting Autumn Soil Freezing". *Remote Sensing of Environment* 180: 346–360. doi:10.1016/j.rse.2016.01.012.

Rodionova, N. V. 2017. "Sentinel-1 Data Correlation with Ground Measurements of Soil Temperature." *Sovremennye Problemy Distantsionnogo Zondirovaniya Zemli Iz Kosmosa* 14 (5): 135–148. doi:10.21046/2070-7401-2017-14-5-135-148.

Rowlandson, T. L., A. A. Berg, A. Roy, E. Kim, R. Pardo Lara, J. Powers, K. Lewis, et al. 2018. "Capturing Agricultural Soil Freeze/Thaw State through Remote Sensing and Ground Observations: A Soil Freeze/Thaw Validation Campaign". *Remote Sensing of Environment* 211: 59–70. doi:10.1016/j.rse.2018.04.003.

Roy, A., Royer, A., Derksen, C., Brucker, L., Langlois, A., Mialon, A., Kerr, Y.H. 2015. "Evaluation of Spaceborne L-band Radiometer Measurements for Terrestrial Freeze/Thaw Retrievals in Canada." *IEEE Journal of Selected Topics in Applied Earth* 8: 4442–4459.

Roy, A., P. Toose, C. Derksen, T. Rowlandson, A. Berg, J. Lemmetyinen, A. Royer, et al. 2017a. "Spatial Variability of L-Band Brightness Temperature during Freeze/Thaw Events over a Prairie Environment". *Remote Sensing* 9: 894. doi:10.3390/rs9090894.

Roy, A., P. Toose, M. Williamson, T. Rowlandson, C. Derksen, A. Royer, A. A. Berg, et al. 2017b. "Response of L-Band Brightness Temperatures to Freeze/Thaw and Snow Dynamics in a Prairie Environment from Ground-based Radiometer Measurements". *In Remote Sensing of Environment* 191: 67–80. doi:10.1016/j.rse.2017.01.017.

Schwank, M., C. Matzler, A. Wiesmann, U. Wegmuller, J. Pulliainen, J. Lemmetyinen, K. Rautiainen, et al. 2015. "Snow Density and Ground Permittivity Retrieved from L-band Radiometry: A Synthetic Analysis." *IEEE Journal of Selected Topics in Applied Earth Observations and Remote Sensing* 8 (8): 3833–3845. doi:10.1109/JSTARS.4609443.

Smith, N. V., S. S. Saatchi, and J. T. Randerson. 2018. "Trends in High Northern Latitude Soil Freeze Thaw Cycles from 1988 to 2002." *Journal of Geophysical Research* 109: 1–14.

UAA. 2019. "Permafrost Laboratory University of Alaska." [Online]. *Database*. http://permafrost.gi.alaska.edu/site/fbw/isa

Vonlanthen, C. M., M. K. Raynolds, C. A. Munger, A. N. Kade, and D. A. Walker. 2005. "Biocomplexity of Patterned Ground Isachsen Expedition." In *AGC Data Report*, 86. Fairbanks, AK: University of Alaska Fairbanks.

Wigneron, J.-P., T. J. Jackson, P. O'Neill, G. De Lannoy, P. de Rosnay, J. P. Walker, P. Ferrazzoli, et al. 2017. "Modelling the Passive Microwave Signature from Land Surfaces: A Review of Recent Results and Application to the L-band SMOS & SMAP Soil Moisture Retrieval Algorithms". *Remote Sensing of Environment* 192: 238–262. doi:10.1016/j.rse.2017.01.024.

WMO World Meteorological organization. October 2015. [Online]. "Status of the Global Observing System for Climate (GCOS-195)." http://www.wmo.int/pages/prog/gcos/Publications/GCOS-195_en.pdf

Xu, X., C. Derksen, R. S. Dunbar, A. Colliander, J. Kimball, and Y. Kim. 2017. "Landscape Freeze/thaw Standard and Enhanced Products from Soil Moisture Active/Passive (SMAP) Radiometer Data." In *IEEE International Geoscience and Remote Sensing Symposium (IGARSS)*, 2550–2553. Fort Worth, TX.

Yi, Y., J. S. Kimball, R. H. Chen, M. Moghaddam, C. E. Miller. 2019. "Sensitivity of Active-layer Freezing Process to Snow Cover in Arctic Alaska." *The Cryosphere* 13 (1): 197–218. doi:10.5194/tc-13-197-2019.

Zhao, T., J. Shi, T. Hu, L. Zhao, D. Zou, T. Wang, D. Ji, et al. 2017. "Estimation of High-resolution Nearsurface Freeze/Thaw State by the Integration of Microwave and Thermal Infrared Remote Sensing Data on the Tibetan Plateau." *Earth and Space Science* 4: 472–484. doi:10.1002/2017EA000277.

Zhao, T., L. Zhang, L. Jiang, S. Zhao, L. Chai, R. Jin. 2011. "A New Soil Freeze/Thaw Discriminant Algorithm Using AMSR-E Passive Microwave Imagery." *Hydrological Processes* 25 (11): 1704–1716. doi:10.1002/hyp.v25.11.